Cross-Sensor Feedback Stabilization of an Emulated Quantum Spin Gyroscope

J.-C. Jaskula,[1] K. Saha,[1,2] A. Ajoy,[1,3] D.J. Twitchen,[4] M. Markham,[4] and P. Cappellaro[1,*]

[1] *Department of Nuclear Science and Engineering and Research Laboratory of Electronics, Massachusetts Institute of Technology, Cambridge, Massachusetts, 02139, USA*

[2] *Department of Electrical Engineering, Indian Institute of Technology Bombay, Mumbai 400 076, India*

[3] *Department of Chemistry, University of California Berkeley, and Materials Science Division, Lawrence Berkeley National Laboratory, Berkeley California, 94720, USA*

[4] *Element Six Innovation, Harwell Campus, Fermi Avenue, Didcot, Oxfordshire OX11 0QR, United Kingdom*

(Received 13 August 2018; revised manuscript received 24 December 2018; published 3 May 2019)

Quantum sensors, such as the nitrogen-vacancy (N-V) color center in diamond, are known for their exquisite sensitivity but their performance over time is subject to degradation by environmental noise. To improve the long-term robustness of a quantum sensor, here we realize an integrated combinatorial spin sensor in the same micrometer-scale footprint, which exploits two different spin sensitivities to distinct physical quantities to stabilize one spin sensor with local information collected in real time via the second sensor. We show that we can use the electronic spins of a large ensemble of N-V centers as sensors of the local magnetic field fluctuations, affecting both spin sensors, in order to stabilize the output signal of interleaved Ramsey sequences performed on the ^{14}N nuclear spin. An envisioned application of such a device is to sense rotation rates with a stability of several days, allowing navigation with limited or no requirement for geolocalization. Our results would enable stable rotation sensing for over several hours, which already reflects better performance than microelectromechanical systems (MEMS) gyroscopes of comparable sensitivity and size.

DOI: 10.1103/PhysRevApplied.11.054010

I. INTRODUCTION

Our quest to understand the fundamental laws of nature and to design ever more advanced technologies requires precise measurements with outstanding performance even in challenging environmental conditions. The realization of breakthrough discoveries and revolutionary technologies, such as gravitational-wave detection and self-driving cars, often implies measuring extremely weak signals, demanding continuous improvement of our measurement tools. Two figures of merit, sensitivity and stability, are crucial for these tasks: while quantum sensors have achieved sensitivities beyond any other technology, they are often prone to instability and decoherence due to external influences. One such quantum sensor is the nitrogen-vacancy (N-V) center in diamond, which is one of the most promising platforms for quantum sensing and many other applications of quantum mechanics [1,2]. Increasing the coherence of N-V centers via better controlled growth of diamonds [3], the implementation of dynamical decoupling sequences [4–6], and quantum memories [7] are just a few of the many advances that have led to an improved magnetic field sensitivity, able to probe nanoscale weak phenomena in condensed matter [8–10] and biology [11]. The measurement of weak signals is, however, not just a matter of using a sensitive device but also of being able to extract signals out of environmental noise via long averaging. In turn, this requires using stable sensors as well as implementing protocols to suppress the effects of different noise sources.

As N-V centers comprise an electronic and a nuclear spin within a single lattice site [12], they enable a broader range of potential applications. Here, we report the design of a compact combinatorial device containing two different large ensembles of sensors in the same footprint, taking advantage of the very high densities (approximately 10^{17} cm^{-3}) of solid-state systems. We demonstrate a cross-sensing application of the N-V electronic and nuclear spin, where the nuclear spin is used as the primary sensor, while the electronic spin, by sensing the exact same fluctuations of the environment, is used to stabilize it. Specifically, we implement Ramsey interferometry with a nuclear spin ensemble, a protocol that could be exploited to make a rotation sensor. The operating principle of such a quantum spin gyroscope is based on the detection of the dynamic phase accumulated due to the rotation of a spin around its symmetry axis [13]. Alternative N-V spin gyroscope designs are based on the measurement of the Berry phase

*pcappell@mit.edu

[14–16], the shift of the Larmor frequency of ^{13}C nuclear spins due to pseudofields [17], or an effective ac magnetic field when the spins are rotating in a noncoaxial static magnetic field [18]. The two latter techniques rely on the ability of the N-V centers to measure their magnetic field environment, which requires the use of highly sensitive N-V electronic spins that suffer from a shorter coherence time compared to the ^{14}N nuclear spins. On the other hand, gyroscopes probing the geometric phase due to the adiabatic evolution of the Hamiltonian during a rotation will have a performance similar to that of devices that measure the dynamic phase. Both can take advantage of using a large number of ^{14}N nuclear spins with a long dephasing time in an isotopically purified ^{12}C diamond to promise rotation sensitivities of the order of $10^{-1}\,\mathrm{deg\,s^{-1}}/\sqrt{\mathrm{Hz}}$ [14–16]. Indeed, because of its small gyromagnetic ratio ($\gamma_N = 0.3$ kHz G^{-1}), the ^{14}N nuclear spin is a poor magnetic field sensor, so it is less perturbed by any magnetic environmental noise and hence exhibits a coherence time of approximately 1 ms in large ensembles.

To improve on that, we pair our rotation-sensing protocol with a feedback loop to reach long-term stability. Typically, feedback protocols such as quantum-error-correction (QEC) codes are implemented via ancilla qubits either for their isolation to the environment or to use redundant degrees of freedom. QEC codes have been proposed with N-V centers for quantum metrology [19,20], where the N-V electronic spin is used as the main sensor and nearby nuclear spins as the ancilla qubits. Here, our approach is the opposite: we rely on the advantages of the nuclear spins as presented above and exploit the fact that the N-V spin is, instead, very sensitive to its environment. We quantify the stability of our quantum sensor in the presence of a controlled magnetic perturbation, in both a free-running and a corrected regime, by computing the Allan deviation, which highlights characteristic features related to the different types of noise affecting our sensors. In particular, we demonstrate, using this figure of merit, that we can stabilize the output signal of the nuclear spins via an active feedback scheme, using the N-V electronic spin as a local magnetic field sensor to monitor the common environment of both spins. We thus recover a square-root behavior of the Allan deviation, enabling an efficient averaging of the nuclear Ramsey signal over a period longer than a day.

II. RESULTS

Our device is based on an ensemble of N-V^- defects in diamond (see Appendix 2), providing a hybrid electron-nuclear-spin system with optical addressability. We design optical and microwave control apparatus, as well as control protocols, in order to demonstrate the capabilities of this sensor. By applying a green laser beam focused on a 10 μm spot during a period of 30 μs, we initialize 10^9 N-V centers in the $m_S = 0$ electronic spin ground-state manifold. Two permanent magnets in a Helmholtz configuration apply a static field of 420 G, aligned along the N-V center's $\langle 111\rangle$ axis. Coherent control between the $m_S = 0$ and $m_S = -1$ spin states is performed via a pulsed resonant microwave at 1.7 GHz. The longitudinal component of the N-V spin state can be determined optically by monitoring the fluorescence intensity with three p-i-n photodiodes placed in contact with the edges of the diamond and thus collecting 6% of the total fluorescence [21].

Electronic spin resonances are optically detected by sweeping the carrier frequency of a 5-μs-long microwave pulse. In Fig. 1(b), we show the spectrum recorded from the ensemble of N-V centers aligned with a magnetic field of 420 G (red) and of 26 G (blue), respectively. The hyperfine coupling between the N-V center and the nitrogen nuclear spin splits each electronic manifold into three nondegenerate states. The relative amplitude of each of the three Lorentzians of the fit provides an estimate of the degree of polarization of the nuclear spin state, which is clearly unpolarized in case of the second spectrum. At a magnetic field of 420 G (corresponding to a Zeeman energy $\gamma_e B \approx 1.18$ GHz), an excited-state level anticrossing (ESLAC) (a zero-field splitting of approximately 1.5 GHz) allows for polarization transfer from the electronic spin onto the nuclear spin [22,23]. This results in the initialization of both N-V-center spins into the $|m_S = 0, m_I = 1\rangle$ state with a polarization of 95(4)%, as is visible in the red spectrum [Fig. 1(b)].

We then choose a pair of hyperfine states ($|0,1\rangle$ and $|0,0\rangle$) as a basis for our sensing qubit, which is coherently controlled using radio-frequency (rf) radiation at 4.68 MHz. The difference between these two state populations is read out by a selective mapping from the state $m_I = 0$ to the $m_S = -1$. Experimentally, we apply a microwave pulse tuned at 1.704 GHz to be resonant on the transition $|0,0\rangle \rightarrow |-1,0\rangle$ before the fluorescence measurement. The spins that were initially in the state $m_I = 0$ will therefore fluoresce with a lower intensity [24]. Our sensing qubit benefits from the longer coherence time of the ^{14}N nuclear spin [25], which is measured by plotting the change of the N-V fluorescence signal F given by Eq. (1) after applying a series of Ramsey pulse sequences (described in Sec. II A). In Fig. 1(d), we observe a decaying signal with a nuclear dephasing time of $T_{2n}^* = 840 \pm 79$ μs.

A. Emulated nuclear spin gyroscope

Using all these steps together, we can implement quantum-sensing protocols to measure various physical quantities. The Ramsey sequence is one simple example of such a protocol, where we drive the nuclear spin sensor to a superposition of states, after which it evolves freely during a precession time t that is usually set on the order of the coherence time T_{2n}^*. It thus acquires a relative phase

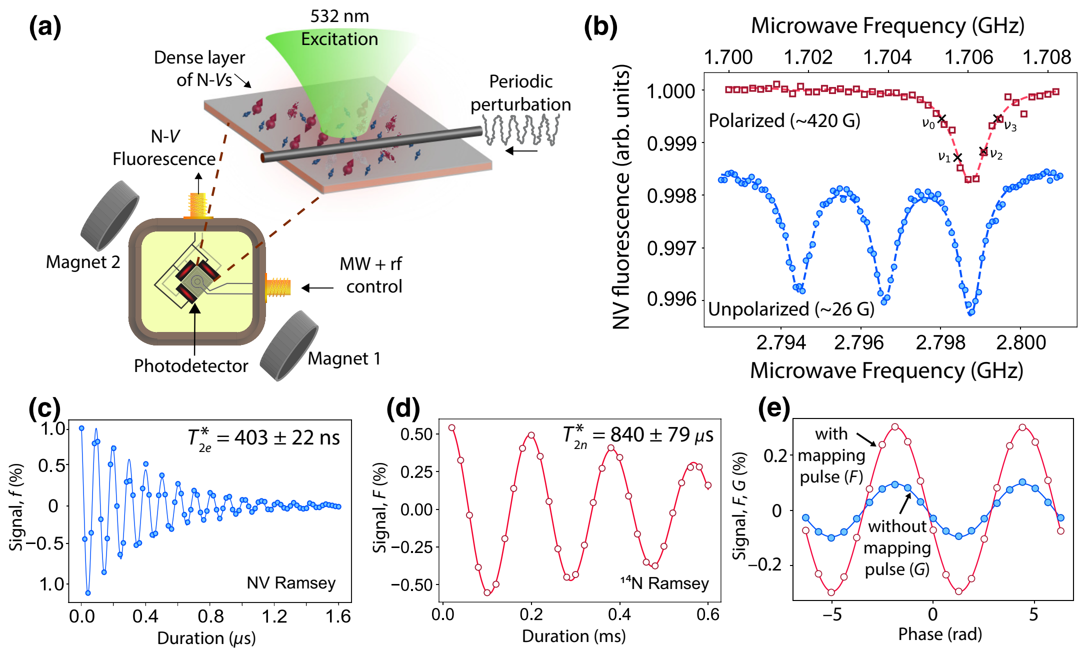

FIG. 1. Control and readout of spin ensembles. (a) Schematics of the experimental device (see the main text for a description). (b) Pulsed electron spin resonance (ESR) spectrum of an ensemble of N-V centers. We use 4 points from a similar pulsed ESR spectrum (as marked on the red curve) to calibrate the N-V spin frequency prior to driving the N-V with the microwave pulses in Fig. 2. The blue curve is offset for better visualization. In blue, the N-V centers are aligned with an external magnetic field of approximately 26 G and show an equal population in each nuclear spin state. On the other hand, for a magnetic field of approximately 420 G (red), the ^{14}N nuclear spin is initialized in a particular spin state ($|m_S = 0, m_I = 1\rangle$) via a transfer of polarization that occurs close to the excited-state level anticrossing (ESLAC). (c) Coherence decay of the electronic spin. We use two subsequent Ramsey sequences, each one composed of two $\pi/2$ pulses detuned from the resonance frequency $\nu_e = 1.704$ GHz by $\Delta\nu_e = 10$ MHz. The phase of the second $\pi/2$ pulses is shifted by π to measure both spin projections. Similarly to Eq. (1), we plot the signal difference f . This signal oscillates at the detuning frequency $\Delta\nu_e$ and decays with a coherence time $T_{2e}^* = 403 \pm 22$ ns. (d) Coherence decay of the nuclear spin. The resonance frequency ν_n is 4.68 MHz and the detuning $\Delta\nu_n = 5.5$ kHz. The nuclear spin is prepared in a superposition of states $(|0,0\rangle + |0,1\rangle)/2$. We measure a coherence time $T_{2n}^* = 840 \pm 79$ μs via a Ramsey pulse sequence. A microwave π pulse tuned at ν_e is used as a selective mapping ($|0,0\rangle \rightarrow |-1,0\rangle$, $|0,1\rangle \rightarrow |0,1\rangle$) between the nuclear spin state and the N-V electronic spin state to obtain higher contrast during the spin-dependent fluorescence readout. (e) Contrast response of the nuclear spin sensor to a linear change of the phase of the last $\pi/2$ pulse of the Ramsey sequence with (without) selective mapping in red (blue, Appendix 3). This is the same response as if the N-V sensor has accumulated a quantum phase Φ during a time $t = 600$ μs due to physical rotation about the N-V axis. The nuclear spin readout can be done without a mapping, releasing the constraint of a narrow-band selective pulse but with lower contrast.

set by the strength of the measured quantity, which is then transferred into a population difference for optical readout. In the case of a rotating spin at a rate Ω and in the presence of an external magnetic field b, the phase is given by $\Phi = (\gamma b + \Omega)t$. In other words, a physical rotation is coupled into this dynamic phase and mapped out through a population difference. Equivalently, and more intuitively, we can consider the two rf $\pi/2$ pulses as being applied along two different axes. The first pulse is along a reference axis (the x axis by convention), while the second one is about an arbitrary axis (the x' axis) that is rotated by an angle $\theta = \Omega t$. In our experimental proof of principle of rotation sensing, we emulate such a phase accumulation by cycling the phase of the last pulse of the Ramsey sequence as shown in Fig. 1(e), followed by a spin readout that includes a mapping pulse (red). Setting the accumulation time $t = 600$ μs close to T_{2n}^*, this sequence simulates a rotation at a rate $\Omega_s = \theta/t$. From a statistical analysis of the data of Fig. 1(e), we determine the rotation-rate sensitivity as the signal amplitude equivalent to the amount of noise $\delta\Omega$ after averaging N_{seq} subsequent sequences during a total acquisition time of 1 s [i.e., the averaged signal for a signal-to-noise ratio (SNR) of 1]. Experimentally, this is measured as $\eta = \sigma_f(T)\sqrt{T}/dS_\Omega$, where σ_f is the standard error in a set of fluorescence signal measurements, T the measurement time, and dS_Ω is the slope of the fluorescence signal as a function of the rotation rate [here, $\Omega = \Phi/t$ from Fig. 1(e)]. We obtain a sensitivity of 3000 $\text{deg}\,\text{s}^{-1}/\sqrt{\text{Hz}}$ for nuclear spins. A sensitivity comparison with electronic spins (sensitivity of 0.5×10^6 $\text{deg}\,\text{s}^{-1}/\sqrt{\text{Hz}}$) indeed shows that the nuclear spin sensor benefits from the longer coherence time. We believe that our sensitivity is reduced by technical limitations that include an excess of electrical noise from the photodetectors as well as an excess of background light from the microwave circuit, which reduces the contrast. We estimate that technical improvements could lead to sensitivities in the order of $10\,\mathrm{deg\,s^{-1}}/\sqrt{\mathrm{Hz}}$ (see Appendix 1). Further improvement can be obtained with dynamical decoupling techniques and spin-bath driving, which would allow for an extension of the coherence time T_2^* [26,27].

Close to the ESLAC, the mechanism of nuclear spin repolarization provides a means of reading out the nuclear spin state without using a narrow-band selective microwave pulse. Indeed, the polarization process is enabled by flip-flops of the electronic and nuclear spins in the excited state. The ensuing state swapping also modifies the measured fluorescence intensity, depending on the initial nuclear state. Such a method has the main advantage of being intrinsic to the N-V center and consequently not relying on any coherent control that requires calibration and stability. However, it suffers from the drawback of lower contrast—here, by a factor of 3 (blue, Fig. 1(e))—as the state swapping is stochastic in nature, due to the 12 ns short excited state lifetime, and not coherent as for the selective pulse.

Our device is built to a very compact design, as nanoscale combinatorial sensors are embedded in the same footprint and coherent control can be delivered by the same loop antenna. Thus, the nuclear and electronic spins allow for measurements of two independent quantities, such as temperature, magnetic and electric fields [28], as well as rotations, probed at the same lattice site. Besides, the two sensors are then sensitive to the same local environment, which could cause errors and drifts of their output signals on different time scales. In particular, in our setup, magnetic field amplitude drifts due to a change of magnetization of the permanent magnets will affect both sensors similarly: a change of magnetic field strength will induce a phase shift during the Ramsey sequence and will cause systematics in the rotation measurement. In the following, we analyze the stability of our combinatorial quantum sensor and describe schemes to mitigate drifts.

Here, we design and implement an adaptive protocol [8,29–31] to locally probe magnetic field changes and feed this information back on both sensors to stabilize their combined output signal. The control protocol is depicted in Fig. 2(a) and consists in six interleaved measurements. We apply a Ramsey sequence to the nuclear spins. The relative phase between the two $\pi/2$ pulses is chosen to be $\theta_r = 90^\circ$ so that the nuclear signal is zero when no phase is accumulated [see Fig. 1(e)]. As described above, a phase shift of the driving field around this ideal bias point mimics a physical rotation that we want to detect. In a regime of small signals, the response of this first sensor will be a linear change of the fluorescence output signal S_{90}, measured with the spin readout, which includes a mapping step as described above. This sensing module is followed by two spin resonance measurements at the frequencies $\nu_4 = \nu + 700$ kHz and $\nu_3 = \nu + 350$ kHz. The second half of the sequence consists in repeating a similar set of measurements with a relative phase $\theta_r = -90^\circ$ and the ESR frequencies $\nu_1 = \nu - 700$ kHz, $\nu_2 = \nu - 350$ kHz. All these frequencies are graphically represented in Fig. 1(b). In a regime where the measured physical quantities are slowly varying with respect to the total sequence length (approximately 1 ms), noise that have a similar signature on both output signals $S_{\pm 90}$—such as laser-intensity noise—can be suppressed by using the effective signal

$$F = \frac{S_{90} - S_{-90}}{S_{90} + S_{-90}}. \tag{1}$$

However, such a common-noise-rejection scheme is still inefficient in the case of noise sources, such as magnetic fields, that act similarly to a signal. To suppress these sources, we exploit the four ESR measurements [32] to probe the line shifts caused by these sources of noise, interleaved with the sensing protocol of the first sensor. The relative fluorescence intensity at four different microwave frequencies allows us to recover the transition frequency ν and determine the strength of the field causing the line shift (see Appendix 2).

In the following, we test our stabilizing schemes against an engineered slowly drifting perturbation generated by applying an oscillating magnetic field created by a coil placed at 1 cm from the diamond sample. Its period is set to 1000 s and its strength along the N-V axis is measured to be 0.14 G peak to peak, via the four-point ESR measurements described above. In Fig. 2(b), a clear oscillation of a period of 1000 s is visible in the signal of the nuclear Ramsey measurements (blue data points) as well as a contribution from a slower environmental noise, over which we have no control, on a time scale of a few hours. While nuclear spins are only slightly sensitive to our applied magnetic perturbation, N-V spins are far more affected by it, which highly disturbs the mapping step. Indeed, the transition frequency of selective pulses must be finely calibrated to maximize the readout fidelity and to be stable over the full measurement data set in order to limit readout errors. However, the feedback protocols that we implement succeed in stabilizing both the nuclear and the electronic spin transition-frequency fluctuations. In what follows, we present two scenarios in which we isolate the effect of the perturbation to a single parameter to be stabilized. First, we compensate the readout mapping pulse frequency to prevent a loss of contrast due to an off-resonance selective pulse. Then, while applying a stronger perturbation but no mapping, we use the signal of the electronic spin to adjust the nuclear spin driving frequency.

B. Cross-sensor feedback stabilization

We demonstrate here that we can use measurements of the local N-V electronic spin to apply feedback on the

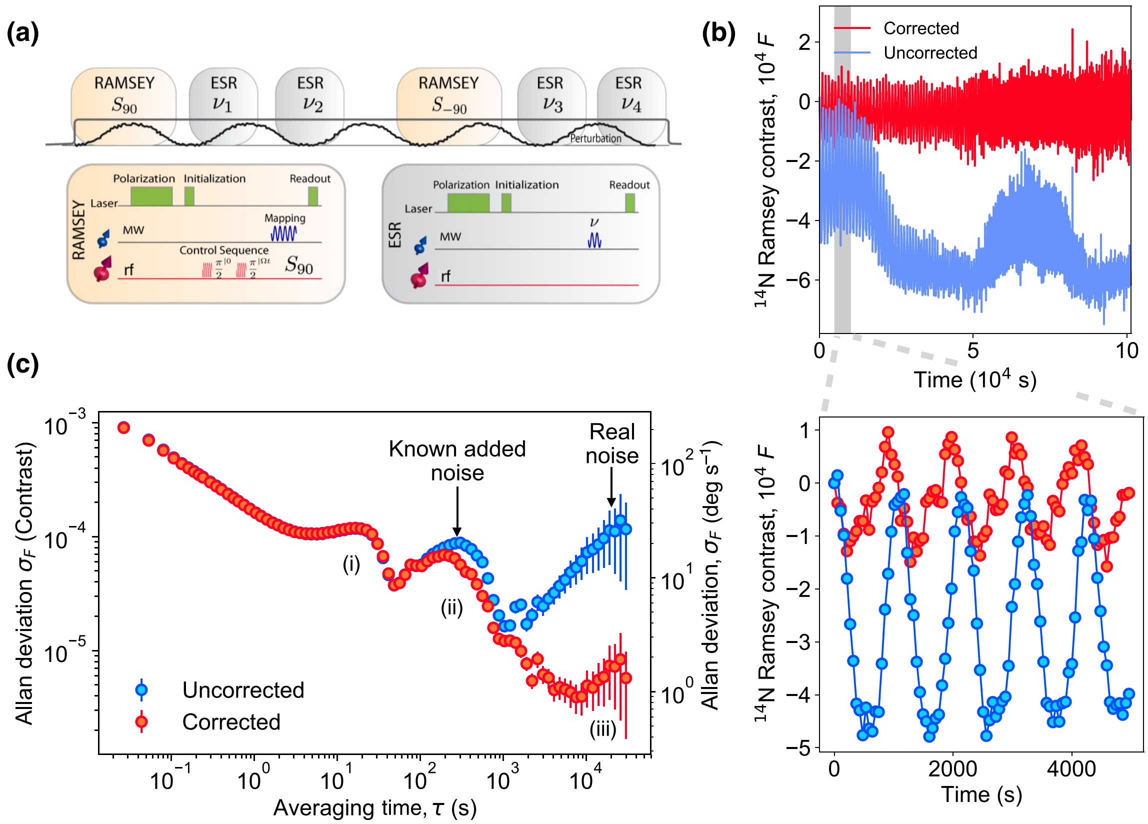

FIG. 2. Nuclear spin sensor with a stabilized readout. (a) The sequence consisting of alternating measurements of the quantum phase via a Ramsey sequence with the ^{14}N nuclear spins ($t = 600\ \mu$s) and measurements of the energy shift via a set of ESR measurements with the N-V spins. The full sequence is symmetrized to reject common noise. (b) Nuclear Ramsey contrast F as defined by Eq. (1) with an uncorrected (blue) and a corrected (red) selective mapping. A slowly varying magnetic field shifts the energy levels and perturbs the mapping. (c) Allan deviations of the Ramsey signals of (b). The maximum averaging time τ used to calculate the Allan deviation is about one third of the total acquisition time of 1.15 d (see Appendix 4). The right-hand axis is rescaled using a factor $s = 4.4 \times 10^6$ (deg s^{-1})$^{-1}$, calculated at the steepest point of curve F in Fig. 1(e).

nuclear Ramsey measurements to stabilize their results. To do that, we (i) repeat the sequence of Fig. 2(a) $N_r = 2000$ times, (ii) transfer the measurements on the control computer to compute the ESR shift, and (iii) update the experimental parameters to compensate the measured magnetic drifts. The two last steps take about 50 s—i.e., a total duration of 1 min—which would optimally set a lower bound for N_r, as one would like to maximize the duty cycle of the sensors. On the other hand, the characteristic time scale and amplitude of the noise limits the number N_r of repetitions after which the correction has to be made as the frequency drift becomes significant. In the case of the engineered perturbation, we choose $N_r = 2000$, as this corresponds to the maximal drift equivalent to one tenth of the Rabi frequency of the mapping pulse and it is smaller than the bandwidth of the ESR measurements (approximately 500 kHz). We show that feedback helps to make the measurement more stable over the full data acquisition of more than 1 d [Fig. 2(b), red].

More quantitatively, we characterize the stability of our dual-spin sensor by computing the Allan deviation of the data traces of Fig. 2(b) [see Appendix 4 and Fig. 2(c)]. We observe that the uncorrected signal (shown in blue) displays an overall decaying behavior with three features. The first two, at $T = 50$ s and $T = 1000$ s, are the signature of periodic noises at frequencies $1/T$. They correspond to perturbations associated with (i) the episodically interrupted recordings to update the experimental parameters and (ii) the magnetic perturbation that we apply to our sensor. The third noticeable feature (iii) is due to the environmental noise that prevents the sensors from operating accurately over long runs. We believe that this is mainly due to temperature changes that affect the magnetization of the permanent magnets. Shown in red is the Allan deviation for the corrected data set, which displays a varying stability improvement on different time scales. Perturbation (ii) is only partially corrected, mainly because of the comparable time scale of the data acquisition (about 1 min) and the magnetic perturbation period (1000 s), so that the measured field has already considerably changed by the time the correction is applied during the next acquisition. This is not the case for the uncontrolled environmental noise (iii), as its variations are much slower: then, the feedback protocol based on monitoring a second spin sensor allows for an improvement of the first sensor readout stability, by an order of magnitude. While in this experiment we limit the feedback correction to the electronic spin driving frequency, we show next that we can obtain additional gain by directly correcting the nuclear spin control.

As both sensors are spins, they are sensitive to magnetic field fluctuations through Zeeman coupling. Due to a small gyromagnetic ratio (10 000 times smaller than that of an electron), the ^{14}N nuclear spin's response to magnetic fluctuations is weaker. Thus, to be able to see the effect of the magnetic perturbation, we increase its strength to a peak-to-peak value of approximately 3 G. At the same time, we lengthen its period to 3000 s to stay within the limit of the previously presented four-point ESR bandwidth. Also, to isolate the effect of the perturbation on the nuclear spins, we extract the signal G directly from the bare fluorescence without any selective mapping [similarly defined as in Eq. (1); see Appendix 3]. We first plot in blue the Allan deviation of the uncorrected signal [Fig. 3(b)]. One can distinguish a small deviation from the expected square-root behavior, confirming that a relative phase due to the magnetic perturbation is imprinted during the free evolution of the nuclear Ramsey sequence.

To correct this, we exploit the fact that the N-V spin can probe the strength of this perturbation with a good accuracy, at exactly the same location, to cross feedback between the two sensors [Fig. 3(a)]. We probe the Zeeman shift $\delta\nu_{\mathrm{N}-V}$ with the four-point ESR scheme and update the driving frequency of the nuclear Ramsey pulses with a frequency shift $\delta\nu_{\mathrm{N}} = -\gamma_{\mathrm{N}}/\gamma_e \delta\nu_{\mathrm{N}-V}$. In addition to the free-running Ramsey sequence (blue), two other data acquisitions are interleaved at the same time with different correction factors: with the correct shift given above (red) and with its opposite (black), thus doubling the error. We can see that we recover stable data averaging for the good feedback correction factor, whereas the opposite correction leads to an amplification of the perturbation, thus proving that the source of noise is indeed the same for the two spins.

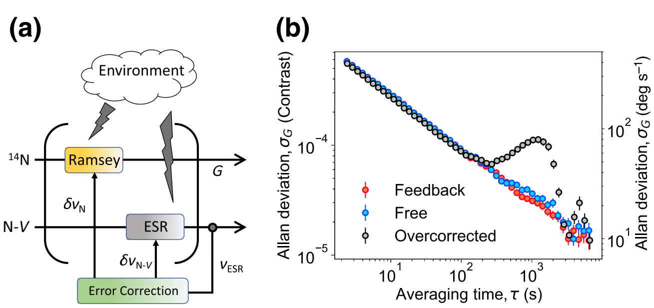

FIG. 3. Stabilized nuclear spin sensor. (a) Dual-sensor scheme. The ESR shift ν_{ESR} collected from the N-V spins also serves to apply feedback on the nuclear spin control parameters $\delta\nu_{\mathrm{N}}$ to stabilize the ^{14}N nuclear Ramsey contrast G with respect to a noise common to both spins. (b) Allan deviation of the nuclear spin signal for different correction strengths. We directly collect the nuclear-spin-state-dependent fluorescence without mapping pulse to isolate the perturbation effect on the nuclear spin signal. The right-hand axis is rescaled using a factor $s = 1.4 \times 10^6\,(\mathrm{deg\,s^{-1}})^{-1}$, calculated at the steepest point of curve G in Fig. 1(e).

C. History-based feedback protocols

So far, our feedback protocol has consisted only in updating the experimental parameters with averaged values recorded during the previous data set. However, as we keep records of every data set, it is in principle possible to use all this knowledge to correct for slower frequency drifts with more advanced protocols. In particular, schemes relying on machine-learning techniques [29,30] or on the Bayesian rule [8] are potential candidates to extract the most important features of the noise and to be able to apply efficient corrections. Here, we would like to assess the question of the efficiency of using the previous records in the presence of stochastic noise to correct the control parameters of an ensemble of sensors. We simulate a signal that is constantly equal to zero (similar to the signal F at the most sensitive operating point), on top of which is added a sinusoidal perturbation and stochastic noise [Fig. 4(a)]. An intuitive approach to guess the best transition frequency at the $(i+1)$th step is to fit the N previous points with a model function and to extrapolate the result to the future point. In the case where the stochastic noise is absent—as, for example, with a perfect readout—a polynomial fit allows for perfect suppression of the perturbation, as long as one suitably increases the degree of the polynomial [Fig. 4(b)]. This is not necessarily true in the scenario of nonzero stochastic noise. As we can notice, for a noise amplitude of the same order as the sinusoidal perturbation, a linear regression between the last two data sets provides a better correction than higher-order polynomials [Fig. 4(c)]. Experimentally, we measure a ratio between the magnetic perturbation and our readout noise of 0.1 [Fig. 4(d)], indicating that we are in the regime in which taking the past evolution of the transition frequency into account does not provide any help in stabilizing our sensors any further.

III. DISCUSSION

We use a large ensemble of N-V centers in diamond to realize a combinatorial dual-spin sensor, providing the capabilities of measuring two physical quantities on the same micrometer-scale footprint and stabilizing one sensor with local information collected in real time via the second sensor. Both sensors are coherently controlled on microsecond time scales with microwave and rf radiation and read out after laser excitation via an efficient fluorescence collection scheme from the side of the diamond

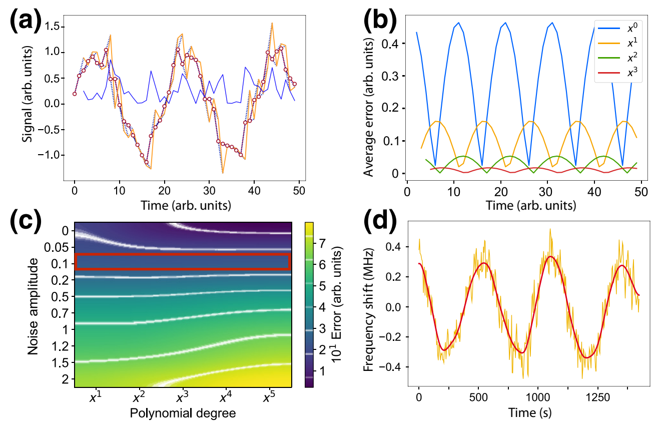

FIG. 4. Simulation of history-based feedback protocols. (a) We simulate a sinusoidal perturbation with stochastic noise of varying amplitude (red). A polynomial (here linear, blue dashed line) fit is used on a certain number N of points $[i, i+N]$ to guess the value of the point $i+N+1$, generating the guessed signal (orange). In blue, we plot the error between red and orange. (b) In the case of the absence of noise, we plot the error as previously defined for different degrees d of the fitting polynomial. The number of points used is set at $N = d+1$. (c) We plot the average error, defined as the mean value of the error [blue curve in (a)] averaged over 20 realizations, as a function of the noise amplitude and the degree of the polynomial. We note that the trend is different depending on the noise amplitude. (d) From experimental ESR data, we estimate a ratio between the magnetic perturbation and our experimental noise of 0.1. This is a regime in which no improvement can be achieved by using the history of the measurements, as one can see in the red region of (c).

[21]. We use ESR measurements to probe the magnetic field fluctuations and stabilize the output signal of interleaved Ramsey sequences performed on the ^{14}N nuclear spin. Moreover, due to the strong interaction between the two spins that make up the N-V center, one can use the electron spin to increase the nuclear spin readout contrast by a factor of 3. In turn, this would increase the rotation-rate sensitivity by the same factor, since the mapping step extends the length of the sequence by only 5 μs and does not affect the duty cycle. On the other hand, this mapping affects the stability of the sensor and prevents averaging beyond a certain number of repetitions. We show that our feedback scheme can improve the stability of the nuclear spin readout and the accuracy of its measurement. In Fig. 2(c), we see that the precision of the measurement tends to degrade after a total acquisition time of approximately $3\tau_{\mathrm{opt}} = 30\,000$ s. At this optimal point, correcting the mapping pulse frequency allows us to improve the precision on the averaged signal by a factor of 2.5, down to a contrast error of 4×10^{-6} (equivalent to a minimum detectable rotation rate of approximately $1\,\mathrm{deg\,s^{-1}}$) and almost reaches the minimum error given by a perfect average of independent measurements, which would have followed a square-root law. Given the experimental parameters—i.e., the total ESR measurement time (2×50 μs) and the time to compute and update the frequency (which can be reduced to less than 5 s)—the stabilization stage does not extend the sequence significantly either and consequently does not affect the sensitivity. Hence we believe that it is beneficial to use both mapping pulses and a stabilization procedure.

We anticipate that such a device can potentially find application as a very stable gyroscope, allowing navigation with limited, or even no need of, remote localization. Existing technologies such as microelectromechanical systems [33] (MEMS) or spin comagnetometers [34,35] are already successful in making sensitive gyroscopes that have thus gained ubiquitous usage in everyday life, from navigation and inertial sensing to rotation sensors in handheld devices and automobiles. Detailed comparisons in terms of sensitivity and stability between different technologies can be find in Refs. [36,37], and [13]. In particular, while commercial gyroscopes achieve typical sensitivities of $0.1\,\mathrm{deg\,s^{-1}}/\sqrt{\mathrm{Hz}}$ in footprints sized at hundreds of microns, their accuracy is strongly affected by drifts after a few minutes of operation, making them unattractive for geodetic applications [38]. On the other hand, our results show sensing capabilities over many hours, confirming the potential of N-V centers in diamond as a competitive modality for such applications. Furthermore, long-term stability is a key figure of merit in the search for discrepancies in the current theories in fundamental physics and long averaging is almost always required in current tests of Lorentz and CPT symmetries, or searches for clues to understand dark matter [39–41].

ACKNOWLEDGMENTS

This work was supported in part by the Office of Naval Research, Award No. N00014-14-1-0804, by the Army Research Office, Award No. W911NF-11-1-0400, and by Skoltech.

J.-C. Jaskula and K. Saha contributed equally to this work.

APPENDIX: EXPERIMENTAL METHODS

All the uncertainties represent the 95% confidence level.

1. Experimental setup

We use a single-crystal electronic-grade ($N < 5$ ppb) diamond substrate, with rectangular dimensions of 2 mm × 2 mm × 500 μm, grown using chemical-vapor deposition (CVD) by Element Six. The 13-μm-thick top-surface N-V sensing layer consists of 99.999% ^{12}C with a ^{14}N concentration of 20 ppm, which has been irradiated with 4.4 MeV electrons with a flux of $1.3 \times 10^{14}\,\mathrm{cm^{-2}\,s^{-1}}$ for 5 h and subsequently annealed in vacuum at 800 °C for 12 h. The density of N-V defects is estimated [11] to be 2×10^{17} cm^{-3}. By illuminating a 10-μm spot by a focused green laser beam, we address about 10^9 spins. The diamond is cut so that the edge faces are perpendicular to the [110] crystal axis and it is clamped using a piece of polyvinyl chloride (PVC) above a single 2-mm-diameter copper loop, patterned on a printed circuit board (PCB). Most fluorescence emitted by N-V centers is guided via total internal reflection to the edges of the diamond chip, where it is detected by three Si *p-i-n* photodiodes (Hamamatsu S8729) that are pressed against the edges of the chip. We glue, on the active area of each photodiode, a high-pass optical filter (>532 nm) designed to block the leakage of excitation light and maximize the fluorescence contrast. The large 2×3.3 mm^2 active area of the photodiodes and the short stand-off distance (< 1 mm) between the sensor and the front of the optical filter ensure that the photodiode is able to collect about 6% of the optical signal over a wide solid angle. The collected fluorescence rate is measured at 5×10^{13} photons/s, which leads to a photon-shot-noise-limited magnetic field sensitivity of the order of 100 pT/$\sqrt{\mathrm{Hz}}$. Increasing the beam size would allow us to collect stronger fluorescence and reach magnetic sensitivities of 1 pT/$\sqrt{\mathrm{Hz}}$ or lower, comparable to those reported in Refs. [1,11], and [21]. Translated in terms of rotation rates, they would be equivalent to sensitivities of $10\,\mathrm{deg\,s^{-1}}/\sqrt{\mathrm{Hz}}$ with electronic spins and $0.1\,\mathrm{deg\,s^{-1}}/\sqrt{\mathrm{Hz}}$ with nuclear spins, because of the longer coherence time. The electrical signal delivered by the photodiodes is amplified by a fast high-speed current amplifier (Femto, DHPCA-100) and recorded using a digital-to-analog converter (DAQ) (National Instruments NI-PCI 6251).

2. Four-point ESR

We devise a scheme to take advantage of the colocation of two sensors in our device by alternating rotation sensing (by Ramsey sequences on the nuclear spins) with transition-frequency detection via the electronic spin. The frequency depends on external environmental factors. Thus, having a real-time estimate of the actual frequency allows for correction of all these parameters.

To achieve a quick estimate of the frequency, we use a 4-point scheme to measure the ESR fluorescence signal at four frequencies ν_{1-4}, which are increasingly ordered with the frequency around the expected value. To maximize the sensitivity to magnetic field changes, we set the microwave power to maximize the contrast while keeping the line width narrow, which results in maximization of the slope of the spectrum profile. The four frequencies are chosen as a trade-off between following the slopes at the steepest point and keeping the bandwidth large enough to track the magnetic field drifts during a complete acquisition window. The new frequency is estimated as the intersection of the two lines passing through the measurement points 1,2 and 3,4, respectively. Once this is determined, we use the information to correct the nuclear spin readout signal (the feedback). In addition, we use this new information to select the best bias point to further measure the microwave frequency for the next time interval.

In this scheme, we assume that it is possible, for example, to stop the rotation during the ESR measurement, so that the frequency estimate only depends on magnetic field variations. If this is not practical, one can still subtract the estimate of the rotation given by the nuclear spin from the measured total phase of the electronic spin (as the rates at which the phase associated with the rotations is acquired are the same, while they are different for magnetic fields, such a scheme would indeed allow us to distinguish between these two effects).

3. Raw data

We plot in Fig. 5 the full data set of the nuclear Ramsey sequence. The nuclear spin readout is realized by collecting directly the fluorescence emitted by the N-V center. Similarly to Eq. (1), we define the nuclear Ramsey contrast as follows:

$$G = \frac{S'_{90} - S'_{-90}}{S'_{90} + S'_{-90}}, \tag{A1}$$

where S'_θ is the Ramsey signal recorded without using the mapping pulse [blue in Fig. 1(e)]. Because of flip-flop interaction at the ESLAC, the fluorescence is modulated depending on the nuclear spin state but at one third of the amplitude S_θ. In Fig. 5, we see an oscillating signal at the set frequency of 0.3 mHz, caused by the external arbitrary magnetic perturbation applied via a 500-turn coil. The field amplitude is measured at approximately 3 G via an ESR made on the N-V electronic spins. This strength, as well as the period, are chosen such that we can notice an effect in the nuclear Ramsey signal while staying within the bandwidth of the 4-point ESR step. Indeed, during the

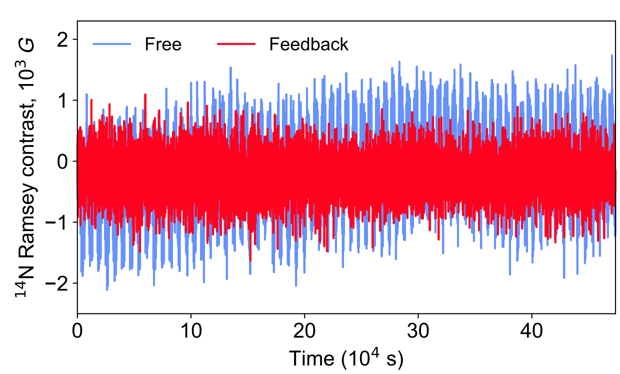

FIG. 5. Nuclear Ramsey signal collected directly from the N-V fluorescence, without mapping from the nuclear to the electronic spin states.

acquisition of the $N_r = 2000$ Ramsey sequences (a total duration of 25 s including dead time), the line shift must stay lower than 350 kHz.

4. Allan deviation

The Allan variance of a signal S is defined as one half of the time average of the squares of the differences between successive readings of the frequency deviation sampled over the sampling period:

$$\sigma^2(\tau) = \frac{1}{2}\left\langle\left(\frac{\Delta_\tau S}{\tau}\right)^2\right\rangle, \qquad \text{(A2)}$$

where $\Delta_\tau S = S(t+\tau) - S(t)$. For a measurement at two intervals separated by τ, the value of $\Delta_\tau S$ will be an indicator of the stability and precision of our sensor over the measured period τ. Indeed, if we repeat this procedure many times, the average value of $(\Delta_\tau S/\tau)^2$ is equal to twice the Allan variance for observation time τ and will carry information about the noise correlations and how they affect the signal-output averaging. The ideal behavior of the Allan deviation is a decay as a square-root law, indicating the absence of correlation between consecutive measurements, which can be then successfully averaged. At long τ, it is experimentally expected that the Allan deviation will start to increase again, suggesting that the signal output is inevitably drifting due to environmental noise and changes, and that further averaging does not improve the SNR. The error bars are directly given the number of subdivisions of the initial full data set and their increase with τ simply reflects the fact that the number of data-set subdivisions becomes inversely small for large τ. Moreover, calculation of an Allan deviation requires a minimum of three subdivisions. Thus, the maximum τ used in Fig. 2(c) (30000 s) is at most one third of the total acquisition time of 10^5 s; i.e., 1 d and 4 h.

[1] T. Wolf, P. Neumann, K. Nakamura, H. Sumiya, T. Ohshima, J. Isoya, and J. Wrachtrup, Subpicotesla Diamond Magnetometry, Phys. Rev. X **5**, 041001 (2015).

[2] C. L. Degen, F. Reinhard, and P. Cappellaro, Quantum sensing, Rev. Mod. Phys. **89**, 035002 (2017).

[3] G. Balasubramanian, P. Neumann, D. Twitchen, M. Markham, R. Kolesov, N. Mizuochi, J. Isoya, J. Achard, J. Beck, J. Tissler, V. Jacques, P. R. Hemmer, F. Jelezko, and J. Wrachtrup, Ultralong spin coherence time in isotopically engineered diamond, Nat. Mater. **8**, 383 (2009).

[4] N. Bar-Gill, L. Pham, A. Jarmola, D. Budker, and R. Walsworth, Solid-state electronic spin coherence time approaching one second, Nat. Commun. **4**, 1743 (2013).

[5] G. de Lange, Z. H. Wang, D. Riste, V. V. Dobrovitski, and R. Hanson, Universal dynamical decoupling of a single solid-state spin from a spin bath, Science **330**, 60 (2010).

[6] H. S. Knowles, D. M. Kara, and M. Atatüre, Observing bulk diamond spin coherence in high-purity nanodiamonds, Nat. Mater. **13**, 21 (2014).

[7] T. Rosskopf, J. Zopes, J. M. Boss, and C. L. Degen, A quantum spectrum analyzer enhanced by a nuclear spin memory, NPJ Quantum Inf. **3**, 33 (2017).

[8] C. Bonato, M. S. Blok, H. T. Dinani, D. W. Berry, M. L. Markham, D. J. Twitchen, and R. Hanson, Optimized quantum sensing with a single electron spin using real-time adaptive measurements, Nat. Nano **11**, 247 (2016).

[9] I. Gross, W. Akhtar, V. Garcia, L. J. Martinez, S. Chouaieb, K. Garcia, C. Carretero, A. Barthelemy, P. Appel, P. Maletinsky, J. V. Kim, J. Y. Chauleau, N. Jaouen, M. Viret, M. Bibes, S. Fusil, and V. Jacques, Real-space imaging of non-collinear antiferromagnetic order with a single-spin magnetometer, Nature **549**, 252 (2017).

[10] L. Rondin, J. P. Tetienne, S. Rohart, A. Thiaville, T. Hingant, P. Spinicelli, J. F. Roch, and V. Jacques, Stray-field imaging of magnetic vortices with a single diamond spin, Nat. Commun. **4**, 2279 (2013).

[11] J. F. Barry, M. J. Turner, J. M. Schloss, D. R. Glenn, Y. Song, M. D. Lukin, H. Park, and R. L. Walsworth, Optical magnetic detection of single-neuron action potentials using quantum defects in diamond, Proc. Natl. Acad. Sci. U.S.A. **113**, 14133 (2016).

[12] M. W. Doherty, N. B. Manson, P. Delaney, F. Jelezko, J. Wrachtrup, and L. C. L. Hollenberg, The nitrogen-vacancy colour centre in diamond, Phys. Rep. **528**, 1 (2013).

[13] A. Ajoy and P. Cappellaro, Stable three-axis nuclear-spin gyroscope in diamond, Phys. Rev. A **86**, 062104 (2012).

[14] D. Maclaurin, M. W. Doherty, L. C. L. Hollenberg, and A. M. Martin, Measurable Quantum Geometric Phase from a Rotating Single Spin, Phys. Rev. Lett. **108**, 240403 (2012).

[15] X. Song, L. Wang, F. Feng, L. Lou, W. Diao, and C. Duan, Nanoscale quantum gyroscope using a single ^{13}C nuclear spin coupled with a nearby NV center in diamond, J. Appl. Phys. **123**, 114301 (2018).

[16] M. P. Ledbetter, K. Jensen, R. Fischer, A. Jarmola, and D. Budker, Gyroscopes based on nitrogen-vacancy centers in diamond, Phys. Rev. A **86**, 052116 (2012).

[17] A. A. Wood, E. Lilette, Y. Y. Fein, V. S. Perunicic, L. C. L. Hollenberg, R. E. Scholten, and A. M. Martin, Magnetic pseudo-fields in a rotating electron-nuclear spin system, Nat. Phys. **13**, 1070 (2017).

[18] A. A. Wood, E. Lilette, Y. Y. Fein, N. Tomek, L. P. McGuinness, L. C. L. Hollenberg, R. E. Scholten, and A. M. Martin, Quantum measurement of a rapidly rotating spin qubit in diamond, Sci. Adv. **4**, eaar7691 (2018).

[19] E. M. Kessler, I. Lovchinsky, A. O. Sushkov, and M. D. Lukin, Quantum Error Correction for Metrology, Phys. Rev. Lett. **112**, 150802 (2014).

[20] T. Unden, P. Balasubramanian, D. Louzon, Y. Vinkler, M. B. Plenio, M. Markham, D. Twitchen, A. Stacey, I. Lovchinsky, A. O. Sushkov, M. D. Lukin, A. Retzker, B. Naydenov, L. P. McGuinness, and F. Jelezko, Quantum Metrology Enhanced by Repetitive Quantum Error Correction, Phys. Rev. Lett. **116**, 230502 (2016).

[21] D. Le Sage, L. M. Pham, N. Bar-Gill, C. Belthangady, M. D. Lukin, A. Yacoby, and R. L. Walsworth, Efficient

photon detection from color centers in a diamond optical waveguide, Phys. Rev. B **85**, 121202 (2012).
[22] V. Jacques, P. Neumann, J. Beck, M. Markham, D. Twitchen, J. Meijer, F. Kaiser, G. Balasubramanian, F. Jelezko, and J. Wrachtrup, Dynamic Polarization of Single Nuclear Spins by Optical Pumping of Nitrogen-Vacancy Color Centers in Diamond at Room Temperature, Phys. Rev. Lett. **102**, 057403 (2009).
[23] R. Fischer, A. Jarmola, P. Kehayias, and D. Budker, Optical polarization of nuclear ensembles in diamond, Phys. Rev. B **87**, 125207 (2013).
[24] P. Neumann, J. Beck, M. Steiner, F. Rempp, H. Fedder, P. R. Hemmer, J. Wrachtrup, and F. Jelezko, Single-shot readout of a single nuclear spin, Science **329**, 542 (2010).
[25] B. Smeltzer, J. McIntyre, and L. Childress, Robust control of individual nuclear spins in diamond, Phys. Rev. A **80**, 1 (2009).
[26] M. Chen, W. K. C. Sun, K. Saha, J.-C. Jaskula, and P. Cappellaro, Protecting solid-state spins from a strongly coupled environment, New J. Phys. **20**, 063011 (2018).
[27] E. Bauch, C. A. Hart, J. M. Schloss, M. J. Turner, J. F. Barry, P. Kehayias, S. Singh, and R. L. Walsworth, Ultralong Dephasing Times in Solid-State Spin Ensembles via Quantum Control, Phys. Rev. X **8**, 031025 (2018).
[28] V. M. Acosta, E. Bauch, M. P. Ledbetter, A. Waxman, L. S. Bouchard, and D. Budker, Temperature Dependence of the Nitrogen-Vacancy Magnetic Resonance in Diamond, Phys. Rev. Lett. **104**, 070801 (2010).
[29] S. Mavadia, V. Frey, J. Sastrawan, S. Dona, and M. J. Biercuk, Prediction and real-time compensation of qubit decoherence via machine learning, Nat. Commun. **8**, 14106 (2017).
[30] R. S. Gupta and M. J. Biercuk, Machine Learning for Predictive Estimation of Qubit Dynamics Subject to Dephasing, Phys. Rev. Appl. **9**, 064042 (2018).
[31] C. Bonato and D. W. Berry, Adaptive tracking of a time-varying field with a quantum sensor, Phys. Rev. A **95**, 052348 (2017).
[32] G. Kucsko, P. C. Maurer, N. Y. Yao, M. Kubo, H. J. Noh, P. K. Lo, H. Park, and M. D. Lukin, Nanometre-scale thermometry in a living cell, Nature **500**, 54 (2013).
[33] H. Johari, J. Shah, and F. Ayazi, in *IEEE 21st International Conference on Micro Electro Mechanical Systems* (IEEE, Wuhan, China, 2008), pp. 856–859.
[34] T. W. Kornack, R. K. Ghosh, and M. V. Romalis, Nuclear Spin Gyroscope Based on an Atomic Comagnetometer, Phys. Rev. Lett. **95**, 230801 (2005).
[35] M. E. Limes, D. Sheng, and M. V. Romalis, ^{3}He $-$ ^{129}Xe Comagnetometery Using ^{87}Rb Detection and Decoupling, Phys. Rev. Lett. **120**, 033401 (2018).
[36] K. Takase, Ph.D. thesis, Stanford University (2008).
[37] V. M. N. Passaro, A. Cuccovillo, L. Vaiani, M. De Carlo, and C. E. Campanella, Gyroscope technology and applications: A review in the industrial perspective, Sensors **17**, 2284 (2017).
[38] C. Jekeli, *Inertial Navigation Systems with Geodetic Applications* (Walter de Gruyter, New York, 2000).
[39] D. Budker, P. W. Graham, M. Ledbetter, S. Rajendran, and A. O. Sushkov, Proposal for a Cosmic Axion Spin Precession Experiment (CASPEr), Phys. Rev. X **4**, 021030 (2014).
[40] A. Garcon, D. Aybas, J. W. Blanchard, G. Centers, N. L. Figueroa, P. W. Graham, D. F. J. Kimball, S. Rajendran, M. G. Sendra, A. O. Sushkov, L. Trahms, T. Wang, A. Wickenbrock, T. Wu, and D. Budker, The Cosmic Axion Spin Precession Experiment (CASPEr): A dark-matter search with nuclear magnetic resonance, Quantum Sci. Technol. **3**, 014008 (2018).
[41] S. Rajendran, N. Zobrist, A. O. Sushkov, R. Walsworth, and M. Lukin, A method for directional detection of dark matter using spectroscopy of crystal defects, Phys. Rev. D **96**, 035009 (2017).